The benefit of using sea ice concentration satellite data products with uncertainty estimates in summer sea ice data assimilation

Q. Yang[1,2], M. Losch[2], S. Losa[2], T. Jung[2,3], L. Nerger[2], T. Lavergne[4]

1. National Marine Environmental Forecasting Center, Beijing, China
2. Alfred Wegener Institute, Helmholtz Centre for Polar and Marine Research, Bremerhaven, Germany
3. University of Bremen, Bremen, Germany
4. Norwegian Meteorological Institute, Oslo, Norway

Correspondence to: Q. Yang (Qinghua.Yang@awi.de)

Abstract

Recently, the European Space Agency Sea Ice Climate Change Initiative (ESA SICCI) released ice concentration data complete with error estimates that depend on space and time. These data are used to in data assimilation experiments that aim at improving summer ice concentration and thickness forecasts in Arctic. The data assimilation system uses the MIT general circulation model (MITgcm) and a local Singular Evolutive Interpolated Kalman (LSEIK) filter. The effect of using sea ice concentration satellite data products with appropriate uncertainty estimates is assessed by three different experiments: in one experiment the SICCI concentration data is used with constant uncertainties; in two further experiments the same SICCI data are included along with their provided uncertainties; they differ only in imposing different minimum uncertainties. Using the observation uncertainties that are provided with the data improves the ensemble mean state of ice concentration compared to using constant data errors, but ice thickness is not affected in a systematic way. Further investigating this lack of impact on the sea ice thicknesses leads us to a fundamental mismatch between the satellite-based radiometric concentration and the modelled physical ice concentration in summer: the passive microwave sensors used for deriving the vast majority of the sea ice concentration satellite-based observations, cannot distinguish ocean water (in leads) from melt water (in ponds). New data assimilation methodologies that fully account or mitigate this mismatch must be designed for successful assimilation of sea ice concentration satellite data in summer melt conditions. In our study, thickness forecasts can be slightly improved by adopting the pragmatic solution of raising the minimum observation uncertainty, to inflate the data error and ensemble spread.

1. Introduction

For the past 30 years, the Arctic sea ice extent and volume consistently decreased in all seasons with a maximum decline in summer (Vaughan et al., 2013). This retreat has large effects on the climate system. For example, the strong contrast between the albedo of sea ice and open water has a profound effect on the Arctic surface heat budget. This retreat also influences the lower-latitude weather and climate, and can be linked to extreme events at mid-latitudes, for example, unusually cold and snowy winters in Europe, the US and Eastern Asia (Liu et al., 2012; Cohen et al., 2012), heat waves and droughts in the US and in Europe (Tang et al., 2014) and anomalous anticyclone circulation over eastern European and Russia (e.g., Semmler et al., 2012; Yang and Christensen, 2012). Apart from its relevance to local and global climate, Arctic sea ice decline opens new economic opportunities. Accurate summer sea ice forecasts are therefore urgently required to thoroughly manage the opportunities (e.g., shipping, tourism) and risks (e.g., oil spill, marine emergencies) associated with Arctic opening (Eicken, 2013).

Sea ice data assimilation (DA) plays a pivotal role in sea ice forecasting, as it can provide realistic initial model states, and continuously constrain the model state closer to reality. Data assimilation requires both reliable observed quantities and realistic uncertainty estimates. These requirements, especially regarding data uncertainties, are now also increasingly recognized by the sea ice remote sensing community. Previous studies have shown that the assimilation of sea ice concentration data can improve sea ice concentration estimates (e.g., Lisæter et al., 2003; Lindsay and Zhang, 2006; Stark et al., 2008; Tietsche et al., 2013; Buehner et al., 2014) and also constrain the ice thickness and volume (Schweiger et al., 2011; Yang et al., 2015a). Given that error

54 estimates in the studies mentioned above were assumed to be constant, there is scope for further improvement
55 through the use of more realistic uncertainty estimates.
56
57 In 2010, the European Meteorological Satellite Agency (EUMETSAT) Ocean and Sea Ice Satellite Application
58 Facility (OSISAF, www.osi-saf.org) released a climate data record of sea ice concentration based on SMMR and
59 SSM/I data (Eastwood et al., 2011; Product OSI-409). This dataset features an explicit correction of the satellite
60 signal due to weather contamination, dynamic adaptation of algorithm tie-points, and spatio-temporally varying
61 maps of uncertainties. In fact, this OSI-409 dataset and its uncertainties were already successfully used for data
62 assimilation purposes (e.g., Massonnet et al. 2013).
63
64 In May 2014, the European Space Agency (ESA)-Sea Ice Climate Change Initiative (SICCI) released a sea ice
65 concentration data set with associated uncertainty estimates (Version 1.11) to the public. In many respects, the
66 SICCI sea ice concentration dataset features an update of the algorithms and processing methodologies used for
67 the OSISAF OSI-409 dataset and, importantly, revised uncertainty estimates (Lavergne and Rinne, 2014). At
68 the time of writing these two datasets, SICCI and OSISAF OSI-409, are the only algorithms or products that
69 come with a physically based sea ice retrieval uncertainty information - as opposed to an estimate of the spatio-
70 temporal variation of the ice concentration within a certain grid area and time window. Besides the SSM/I time-
71 series covering from 1992 to 2008, SICCI (v1.11) also includes sea ice concentration maps from AMSR-E (2002-
72 2011). This new data set provides an opportunity to study the effect of the revised local (i.e., spatially varying)
73 uncertainties on the assimilation of sea ice concentration data, and hence sea ice prediction skill.
74
75 In this study, we follow the approach of Yang et al. (2015a) and Yang et al. (2015b) by focusing on the summer
76 of 2010 and using the same ensemble-based Singular Evolutive Interpolated Kalman (SEIK) filter (Pham et al.,
77 1998; Pham, 2001) in its local form (LSEIK, Nerger et al., 2006). The SEIK filter algorithm is selected to
78 assimilate the sea ice concentration because it is computationally efficient when applied to nonlinear models
79 (Nerger et al., 2005), and the LSEIK filter has already been successfully used for the sea ice concentration data
80 assimilation (Yang et al., 2015a). The purpose of the study is to quantify the impact of different uncertainty
81 approximations on sea ice data assimilation through a comparison with independent ice concentration and ice
82 thickness observations.
83
84 **2. Forecasting experiment design**
85 We use the MITgcm sea ice-ocean model (Marshall et al., 1997; Losch et al., 2010; Losch et al., 2014). Following
86 Yang et al. (2015a) and Yang et al. (2015b), this study employs an Arctic regional configuration with a horizontal
87 resolution of about 18 km and open boundaries in the North Atlantic and North Pacific (Losch et al., 2010;
88 Nguyen et al., 2011). To explicitly include flow dependent uncertainty in atmospheric forcing, the approach by
89 Yang et al. (2015a) was used in which UK Met Office (UKMO) ensemble forecasts from the TIGGE archive
90 (THORPEX Interactive Grand Global Ensemble; http://tigge.ecmwf.int/) drive the ensemble of sea ice-ocean
91 models. Each of the selected UKMO ensemble forecasts consists of one unperturbed 'control' forecast and an
92 ensemble of 23 forecasts with perturbed initial conditions. For further details the reader is referred to Bowler et
93 al. (2008) and Yang et al. (2015a).
94
95 Following Yang et al. (2015a) and Yang et al. (2015b), the system's forecasting skills are evaluated with a series
96 of 24h forecasts over the period of 1 June to 30 August 2010 during which the LSEIK filter is applied every day.
97 This particular period is chosen as the open water was first found in the interior pack ice near the North Pole as
98 early as 12 July 2010 (NSIDC, http://nsidc.org/arcticseaicenews/2010/07/). During this summer melting period
99 the Arctic sea ice extent (area with at least 15% sea ice concentration) shrank from 11.8 million km^2 on 1 June
100 to 5.3 million km^2 on 30 August 2010 (data from NSIDC), which shows a clear picture of sea ice melting in
101 Arctic summer: on 1 June, most of the Arctic Ocean was covered with closed ice pack, while on 30 August, the
102 sea ice area was shrunk to the central Arctic and the concentration was also much reduced (Fig. 1).
103
104 The simulated and satellite observed sea ice concentration are combined using a sequential SEIK filter with
105 second order exact sampling (Pham et al., 1998; Pham, 2001) coded within the Parallel Data Assimilation
106 Framework (PDAF, Nerger and Hiller, 2013; http://pdaf.awi.de). The filter algorithm includes the following

phases: initialization, forecast, analysis and ensemble transformation. The sequence of forecast, analysis and ensemble transformation is repeated.

The required initial ensemble approximates the uncertainty in the initial state of the physical phenomena. Following Losa et al. (2012) and Yang et al. (2015a), we used a model integration driven by the 24-h UKMO control forecasts over the period of 1 June to 31 August 2010 to estimate the initial state error covariance matrix of sea ice concentration and thickness. The leading Empirical Orthogonal Functions (EOFs) of this covariance matrix representing the model variability are transformed by the second-order exact sampling to generate the initial ensemble of ice concentration and thickness. An ensemble size of 23 states is chosen to match with the ensemble size of UKMO perturbed forcing. In the forecast phase, all ensemble states are dynamically evolved in time with the fully nonlinear sea ice model driven by the UKMO ensemble atmospheric forcing. The analysis step combines the predicted model state with the observational information and computes a corrected state every 24 hours. The error covariance matrix and ensemble of model state are also updated. With the SEIK filter as a reduced-rank square-root approach, the updated ensemble samples the analyzed model uncertainties according to the leading EOFs.

The SEIK analysis is performed locally for each water column of the model surface grid by assimilating the observational information only within a radius of 126 km (~7 model grid points). Within the radius, we weighted the observations assuming quasi-Gaussian (Gaspari and Cohn, 1999) dependence of the weights on the distance from the analyzed grid point (see Janjić et al., 2012, Losa et al., 2012). As the atmospheric errors are already explicitly accounted for by the ensemble forcing, an ensemble inflation simulating model errors is not needed in this LSEIK configuration (Yang et al., 2015a).

Two daily sea ice concentration data sets are used in this study. The SICCI fields from AMSR-E (Lavergne and Rinne, 2014; http://icdc.zmaw.de/projekte/esa-cci-sea-ice-ecv0.html) are used in the data assimilation. This product consists of daily fields provided on a 25 km polar-centered EASE2 grid (Brodzick et al. 2012). In the SICCI data set, the North Pole data gap is filled by interpolation, and daily maps of total standard error (the sum of algorithm uncertainties and smear uncertainties which refers to the representative error on a different grid resolution) are provided. The ice concentration data used for comparison are from the National Snow and Ice Data Center (NSIDC; Cavalieri and others, 2012; http://nsidc.org/data/docs/daac/nsidc0051_gsfc_seaice.gd.html). This product also consists of daily fields with 25 km grid spacing on a polar stereographic projection. For summer 2010, the NSIDC ice concentration fields are derived from a different passive microwave instrument (SSMIS onboard DMSP F-17) and with a different algorithm (NASA-Team). We note that both the SICCI and NSIDC products are computed from channel combinations of relatively similar passive microwave instruments and that they cannot be regarded as strictly independent. Using a different instrument and a different algorithms is nevertheless often the best we can use for passive microwave sea ice concentration data.

Currently, satellite-based observations of ice thickness are a challenge (Kwok and Sulsky, 2010; Kern et al. 2015), and there are very few reliable summer sea-ice thickness products available. Instead of remote-sensing data we compare our simulation results to measurements of sea ice draft from the Beaufort Gyre Experiment Project (BGEP) Upward Looking Sonar (ULS) moorings located in the Beaufort Sea (BGEP_2009A, BGEP_2009D; http://www.whoi.edu/beaufortgyre; see Fig. 1 for the locations). The error in ULS measurements of ice draft is estimated as 0.1 m (Krishfield and Proshutinsky, 2006). Following Rothrock et al. (2008), drafts are converted to thickness by multiplying by a factor of 1.1. It should be noted that different ice types have different effects on the draft-thickness conversion, as we have not any information of ice types so these effects are ignored in this study.

Three experiments, which mainly differ in the way uncertainties are represented, form the backbone of this study:
1. LSEIK-1: SICCI sea ice concentration data are assimilated with a constant uncertainty value of 0.25, e.i., the observation errors are assumed to be Gaussian distributed with standard deviations (STD) of 0.25.
This constant uncertainty value is larger than the measurement error to account for a representation error which due to the used projection of the observation to the model space.

160
161 2. LSEIK-2: Same as LSEIK-1 but using the uncertainty fields provided with the SICCI product (see Figure 2).
162 A minimum uncertainty of 0.01 is imposed to avoid complications due to divisions by very small numbers.
163 3. LSEIK-3: Same as LSEIK-2, but with a minimum uncertainty of 0.10.
164
165 To reflect the uncertainties in the interpolated or possibly less accurate sea ice concentration data from SICCI
166 (e.g., over the data-void North Pole), a constant uncertainty of 0.30 is assigned in these regions for all
167 experiments.
168
169 The original observational data uncertainties of ice concentrations that are provided with the SICCI data set and
170 used in LSEIK-2 and LSEIK-3 are displayed in Fig. 2. In Fig 2, we show the provided observation uncertainties
171 on 1 June, 16 June, 1 July, 16 July, 1 August and 16 August 2010. The uncertainties are about 0.05 over packed
172 ice and open water, but larger uncertainties up to and beyond 0.3 are present at the ice edge, and region of
173 intermediate ice concentration values. The SICCI total uncertainties are indeed the sum of two components, one
174 characterizing the algorithm uncertainties, and the other measuring the uncertainties due to representativity of
175 25 km daily averages, geo-location and instrument foot-print mismatch (Lavergne and Rinne, 2014). The second
176 component to the total uncertainties is only pronounced in areas of gradients in the sea ice concentration
177 observations – typically at the ice edge –, and amount for the inability of such coarse resolution satellite
178 observations to accurately locate sea ice edge. Should the SICCI sea ice concentrations be assimilated in models
179 with significantly better spatial resolution, the enlarged uncertainties allow the model to freely locate its ice edge
180 within the 25×25 km grid cells showing intermediate ice concentration values in the data.
181
182 **3. Results**
183 Figure 3 compares the root mean square error (RMSE) for ensemble mean ice concentration forecasts with and
184 without data assimilation with respect to the assimilated SICCI (Fig. 3a) and the non-assimilated NSIDC (Fig.
185 3b) ice concentration for the period 1 June to 30 August 2010. Note that Fig. 3 reports only the RMSE for grid
186 location where the satellite products reports and ice concentration lower than 0.35. These are thus mostly location
187 along the ice edge. Fig. 3 thus mostly assesses how the data assimilation experiments constrain the envelope of
188 Arctic sea ice, not the interior (cyan color on Fig. 1). The reason for choosing this range is that all sea ice
189 concentration products from passive microwave instruments have challenges with high concentration values in
190 the summer (Ivanova et al., 2015). In such a case, documenting that the assimilated state is closer to the NSIDC
191 product is not very conclusive, since NSIDC and SICCI products are probably likewise challenged at high
192 concentration values. Looking away from the ice concentration values and focusing on the outskirt of the sea ice
193 cover make the conclusions somewhat more robust as the influence of melt-ponds is reduced, and the approaches
194 over open water are different in both products (weather filters in NSIDC and explicit correction for atmosphere
195 perturbations for SICCI). It should be also noted that for this comparison, the observations are linearly
196 interpolated to the model grids. Such interpolation could lead to small local changes in sea ice concentration,
197 and the related biases are not discussed in this study.
198
199 All the data assimilation experiments reduce deviations of the forecasted ice concentration from the satellite-
200 based data sets. The RMSE temporal evolutions are associated with the number of available data points that can
201 be used for comparison or with surface forcing. Compared to the free run without data assimilation, mean RMSE
202 of LSEIK-1, LSEIK-2 and LSEIK-3 ensemble mean forecasts with respect to the SICCI data are reduced from
203 on average, 0.56 to 0.18, and 0.07, 0.16, respectively. Similarly, the RMSE with respect to the NSIDC data are
204 reduced from 0.55 to 0.20, 0.13 and 0.19. At all times, LSEIK-2 and LSEIK-3, using the SICCI-provided
205 uncertainty estimates and adjusted minimum uncertainties, agree better with both the assimilated SICCI and non-
206 assimilated NSIDC observations than LSEIK-1, which employs a constant uncertainty. Furthermore, it is worth
207 pointing out that LSEIK-2, with the SICCI-provided uncertainties, agrees best with both SICCI and NSIDC
208 observations. This shows that the forecasting system produces a better ensemble mean state for sea ice
209 concentration when the full range of uncertainties provided with the satellite observations are used.
210
211 The time series of daily 24-hr forecast of sea ice thickness are compared to in-situ ULS-observations
212 BGEP_2009A (Fig. 4a) and BGEP_2009D (Fig. 4b). Note, that the numerical model carries mean thickness

213 (volume over area) as a variable. The observed thickness is multiplied by SICCI or NSIDC local ice
214 concentration to arrive at the observed ULS-SICCI or ULS-NSIDC mean thicknesses shown in Fig. 4. Although
215 there are some small differences between ULS-SICCI or ULS-NSIDC, both reveal a very similar variation: At
216 BGEP_2009A, the mean thickness on 1 June was about 2.5m. With ice melting, the thickness was rapidly
217 reduced in July, and reached about 0.2m on 30 August (Fig. 4a). Similarly, the mean thickness at BGEP_2009D
218 was about 3.5m on 1 June and was reduced to less than 0.1m on 30 August (Fig. 4b). All forecasts with data
219 assimilation show improvements over the free-running MITgcm after late July. The ice thickness RMSE with
220 respect to ULS-SICCI at BGEP_2009A has been reduced from 0.86m in the free model run to 0.43m in LSEIK-
221 1, 0.61m in LSEIK-2, and 0.43 m in LSEIK-3 (Table 1). Similarly, the RMSE with respect to ULS-SICCI at
222 BGEP_2009D has been reduced from 0.93m in the free model run to 0.55m in LSEIK-1, 0.51m in LSEIK-2,
223 and 0.59m in LSEIK-3 (Table 1). By using the original SICCI uncertainty, LSEIK-2 gives a good agreement
224 with the in-situ observations at BGEP_2009D (Fig. 4b), but over-estimates the mean sea ice thickness at
225 BGEP_2009A (Fig. 4a), especially from mid-July to mid-August. By imposing a minimum uncertainty of 0.10
226 in the original uncertainties, the LSEIK-3 thickness agrees better with the BGEP_2009A data, and is basically
227 equivalent to LSEIK-1. The reason is discussed in the following section.
228
229 **4. Discussion**
230 Based on the recently released SICCI sea ice concentration data that provides uncertainty estimates, a series of
231 sensitivity experiments with different data error statistics have been carried out to test the impact of sea ice
232 concentration uncertainties in data assimilation. Compared to a data assimilation configuration with constant
233 uncertainty of 0.25, the data assimilation of SICCI data with provided uncertainties can give a better short-range
234 ensemble mean forecasts for sea ice concentration in summer. For ice thickness forecasts the influence of
235 observational uncertainties is ambiguous (beneficial in one case while seemingly detrimental in another). As
236 there is still no available satellite based sea ice thickness data in summer, the ice thickness validation in this
237 study are only based on two local ULS based observations. Also because we calculate the mean ice thickness
238 using the local SICCI or NSIDC sea ice concentration data which is not real and certainly has potential bias, this
239 introduces further uncertainties to the thickness calculations.
240
241 The main message from Fig. 3 is in fact the high sensitivity of the data assimilation to the observation
242 uncertainties can be explained by the employed (atmospheric) model and data error statistics in the LSEIK
243 assimilation system. Although we have not directly included the model errors due to the possible suboptimal sea
244 ice internal parameters, the ensemble forcing approach used here was shown to be very effective at representing
245 model uncertainty associated with atmospheric forcing fields (Yang et al. 2015a). Given this high sensitivity,
246 and given that observation uncertainties that are prescribed by data assimilation teams (LSEIK-1 and LSEIK-3)
247 perform worse than observation uncertainties derived by the data producers, Fig. 3 clearly supports that data
248 providers do compute and deliver data uncertainties along with their products.
249
250 The ensemble-represented standard deviations (STDs) of sea ice concentration for LSEIK-2 turn out to be
251 relatively small. For example, on 30 August 2010, most of the STDs in the Arctic central area and the sea ice
252 edge area are less than 0.01 and 0.03, respectively (Fig. 5c). This means that all members are very close to the
253 ensemble mean and the data assimilation will have only little effect. LSEIK-3 has a similar spread distribution
254 pattern of higher STDs in the sea ice edge area and lower STDs in the concentrated central ice area but overall
255 higher STDs than LSEIK-2. Together with the fact that LSEIK-2 does not fit the thickness observations as well
256 as LSEIK-3, this suggests that the ensemble forecast spread for sea ice concentration is too low and cannot reflect
257 the uncertainty. As only observations of sea ice concentration are assimilated, sea ice thickness is influenced
258 indirectly during the data assimilation through the point-wise covariance between the ice concentration and
259 thickness, thus through a linear update. Here, the very small sea ice concentration variance leads to a very small
260 sea ice thickness spread (Fig. 6b). This probably explains why the LSEIK-2 system is not very effective at
261 improving the sea ice thickness estimates while LSEIK-3 does somewhat better. The increased spread in the sea
262 ice concentration allows the system to better represent the uncertainties and leads to a larger ice thickness spread
263 (Fig. 6c). The sea ice thickness forecasts are improved accordingly.
264

The relative enhanced skill of sea ice thickness forecasts by LSEIK-3 with respect to LSEIK-2, does thus point to a possible issue with assimilating the summer SICCI ice concentration with the provided uncertainties. At first sight, the data uncertainties in summer sea ice pack seem to be too low (Fig. 2). For example, on 16 July 2010 when surface ice melting prevails and the microwave radiometry based ice concentration estimates are known to underestimate the physical sea ice cover (Ivanova et al. 2015), the provided uncertainties at the sea ice pack area are still lower than 0.06 with few regions exhibiting values around 0.1 (Fig. 2d).

In fact, Ivanova et al., (2015, section 5.3 "Melt ponds") report that AMSR-E and SSM/I, like all other passive microwave sensors, cannot distinguish ocean water (in leads) from melt water (in ponds) because of the very shallow penetration depths of the microwave signal in water. Therefore, these radiometric sea ice concentrations are closer to one minus the open water fraction (ponds and leads), than to the physical sea ice concentration in our models. This mismatch between the observed and modelled ice concentration (radiometric vs. physical) does not exist in winter when there is no surface melting. But in summer melt conditions, the observed ice concentration includes an unknown area of pond water. The provided uncertainties are not larger since the radiometric concentration is not more uncertain. This mismatch results in a systematic difference between the two quantities (the physical concentration is larger than the radiometric concentration) that cannot be fully mitigated by enlarged standard deviations of a Gaussian uncertainty model in Ivanova et al. (2015). The influence of melt-ponds on the accuracy of the SICCI dataset is documented in Lavergne and Rinne (2014, section 2.2.1.1 "summer melt-ponding").

This mismatch between the measured and modelled quantities calls for adopting more advanced data assimilation methodologies, e.g. embedding a matching relation in form of an observation operator, that would necessarily include modelled melt pond fraction, for successful assimilation of sea ice concentration satellite observations (from passive microwave instruments). Given the scope of this study and the comparisons with the in-situ BGEP ice thickness, the solution implemented in LSEIK-3, that is to enlarge the observation uncertainties using a minimum value of 0.10, is a pragmatic but effective approach.

5. Conclusion
In this study, we assimilate the summer SICCI sea ice concentration data taking into account the data uncertainties provided by the distributors. Even with a constant data uncertainty for the SICCI data, comparing the assimilated SICCI and non-assimilated NSIDC ice concentration and BGEP in-situ thickness data, its assimilation results in better estimates of the sea ice concentration and thickness. The estimates are further improved when the SICCI-provided uncertainty estimates are taken into account.

However, it was found that our data assimilation system cannot give a reasonable ensemble spread of sea ice concentration and thickness if we use the provided uncertainty directly. This is because 1) there is a mismatch between the summer sea ice concentration as observed by the passive microwave sensors (radiometric concentration) and that simulated by our model (physical concentration), and 2) the provided observation uncertainties are not enlarged to accommodate this mismatch. A simple and pragmatic approach appears to bypass this by imposing a minimum threshold value on the provided uncertainties in summer. Fully resolving the mismatch calls for more research, for example by considering melt-pond cover and evolution in the models, and using observation operators in the data assimilation schemes.

References

Bowler, N., Arribas, A., Mylne, K., Robertson, K., Beare, S.: The MOGREPS short-range ensemble prediction system. Q. J. R. Meteorol. Soc., 134: 703–722, doi: 10.1002/qj.234, 2008.

Brodzik, M. J., Billingsley, B.,, Haran, T., Raup, B., Savoie, M. H.: EASE-Grid 2.0: Incremental but Significant Improvements for Earth-Gridded Data Sets. ISPRS International Journal of Geo-Information, 1(1):32-45, doi:10.3390/ijgi1010032, 2012.

Buehner, M., Caya, A., Carrieres, T., Pogson, L.: Assimilation of SSMIS and ASCAT data and the replacement of highly uncertain estimates in the Environment Canada Regional Ice Prediction System, Q. J. R. Meteorol. Soc., doi:10.1002/qj.2408, 2014.

Cavalieri, D. J., Parkinson C. L., DiGirolamo, N. and Ivanoff, A.: Intersensor calibration between F13 SSMI and F17 SSMIS for global sea ice data records, IEEE Trans. Geosci. Remote Sens., 9(2), 233-236, 2012.

Cohen, J. L., Furtado, J. C., Barlow, M. A., Alexeev, V. A., and Cherry, J. E.: Arctic warming, increasing snow cover and widespread boreal winter cooling, Environ. Res. Lett., 7 (1), 014007, 2012.

Comiso, J. C.: Characteristics of Arctic winter sea ice from satellite multispectral microwave observations, J. Geophys. Res., 91(C1): 975-994, doi: 10.1029/JC091iC01p00975, 1986.

Eastwood, S., Larsen, K. R., Lavergne, T., Neilsen, E. and Tonboe, R.: OSI SAF global sea ice concentration reprocessing: product user manual, version 1.3. EUMETSAT OSI SAF (Product 0SI-409), 2011.

Eicken, H.: Ocean science: Arctic sea ice needs better forecasts, Nature, 497(7450), 431-433, 2013.

Gaspari, G., and Cohn, S. E.: Construction of correlation functions in two and three dimensions, Quart. J. Roy. Meteor. Soc., 125(554), 723-757, 1999.

Ivanova, N. and co-authors.: Satellite passive microwave measurements of sea ice concentration: an optimal algorithm and challenges, The Cryosphere Discuss., 9, 1269-1313, 2015 (accepted for publication in TC).

Janjić, T., Nerger, L., Albertella, A., Schröter, J., Skachko, S.: On domain localization in ensemble based Kalman filter algorithms, Mon. Weather Rev., 139, 2046–2060, 2011.

Kern, S., Khvorostovsky, K., Skourup, H., Rinne, E., Parsakhoo, Z. S., Djepa, V., Wadhams, P., and Sandven, S.: The impact of snow depth, snow density and ice density on sea ice thickness retrieval from satellite radar altimetry: results from the ESA-CCI Sea Ice ECV Project Round Robin Exercise, The Cryosphere, 9, 37-52, doi:10.5194/tc-9-37-2015, 2015.

Krishfield, R. and Proshutinsky, A.: BGOS ULS Data Processing Procedure Report, http://www.whoi.edu/fileserver.do?id=85684pt=2p=100409, Woods Hole Oceanographic Institute, 2006.

Kwok, R and Sulsky, D. : Arctic Ocean sea ice thickness and kinematics: satellite retrievals and modeling. Oceanography, 23(4), 134–143, 2010.

Lavergne, T. and Rinne, E.: Sea Ice Climate Change Initiative Phase 1: D3.4 Product User Guide (PUG), version 2.0. Ref: SICCI-PUG-13-07, 2014.

Lindsay, R. W. and Zhang, J.: Assimilation of ice concentration in an ice-ocean model, J. Atmos. Oceanic Technol., 23(5), 742-749, 2006.

Lisæter, K. A., Rosanova, J. and Evensen, G.: Assimilation of ice concentration in a coupled ice–ocean model, using the Ensemble Kalman filter, Ocean Dyn., 53(4), 368-388, 2003.

Liu, J., Curry, J. A., Wang, H., Song, M., and Horton, R. M.: Impact of declining arctic sea ice on winter snowfall, Proc. Natl. Acad. Sci. U.S.A., 109(11):4074-9., doi: 10.1073/pnas.1114910109, 2012.

Losa, S., Danilov, S., Schröter, J., Nerger, L., Maßmann, S., and Janssen, F.: Assimilating NOAA SST data into the BSH operational circulation model for the North and Baltic Seas: Inference about the data, J Marine. Syst., 105-08, 152-162, 2012.

Losch, M., Menemenlis, D., Campin, J. M., Heimbach, P. and Hill, C.: On the formulation of sea-ice models. Part 1: Effects of different solver implementations and parameterizations, Ocean Modell., 33(1), 129-144, 2010.

Losch, M., Fuchs, A., Lemieux, J., and A. Vanselow: A parallel Jacobian-free Newton-Krylov solver for a coupled sea ice-ocean model, J. Comp. Phys., 257(A), 901-911, doi:10.1016/j.jcp.2013.09.026, 2014.

Marshall, J., Adcroft, A., Hill, C., Perelman, L. and Heisey, C.: A finite-volume, incompressible Navier Stokes model for studies of the ocean on parallel computers, J. Geophys. Res., 102(C3), 5753-5766, 1997.

370   Massonnet, F., Mathiot, P., Fichefet, T., Goosse, H., König Beatty, C., Vancoppenolle, M., and Lavergne, T.: A
371   model reconstruction of the Antarctic sea ice thickness and volume changes over 1980–2008 using data
372   assimilation, Ocean Modell., 64, 67-75, 2013.
373   Nerger, L., Hiller, W. and Schröter, J.: A comparison of error subspace Kalman filters, Tellus A, 57(5), 715-735,
374   2005.
375   Nerger, L., Danilov, S., Hiller, W. and Schröter, J.: Using sea-level data to constrain a finite-element primitive-
376   equation ocean model with a local SEIK filter, Ocean Dyn., 56(5-6), 634-649, 2006.
377   Nerger, L. and Hiller, W.: Software for ensemble-based data assimilation systems—Implementation strategies
378   and scalability, Comp. & Geosci., 55, 110-118, 2013.
379   Nguyen, A. T., Menemenlis, D. and Kwok, R.: Arctic ice-ocean simulation with optimized model parameters:
380   Approach and assessment, J. Geophys. Res., 116(C4), C04025, doi:10.1029/2010JC006573, 2011.
381   Pham, D. T., Verron, J., and Gourdeau, L.: Singular evolutive Kalman filters for data assimilation in
382   oceanography, C. R. Acad. Sci. Paris, Earth Planet. Sci. , 326, 255-260, 1998.
383   Pham, D.: Stochastic methods for sequential data assimilation in strongly nonlinear systems, Mon. Weather Rev.
384   129: 1194–1207, 2001.
385   Rothrock, D. A., Percival, D. B., and Wensnahan, M. : The decline in arctic sea-ice thickness: Separating the
386   spatial, annual, and interannual variability in a quarter century of submarine data, J. Geophys. Res.,
387   113, C05003, doi:10.1029/2007JC004252, 2008.
388   Semmler, T., McGrath, R., and Wang, S.: The impact of Arctic sea ice on the Arctic energy budget and on the
389   climate of the Northern mid-latitudes, Clim. Dyn., 39, 2675–2694, doi:10.1007/s00382-012-1353-9,
390   2012.
391   Smith, D. M. Extraction of winter total sea-ice concentration in the Greenland and Barents Sea from SSM/I data,
392   Int. J. Remote Sens., 17(3): 2625–2646, doi: 10.1080/01431169608949096, 1996.
393   Stark, J. D., Ridley, J., Martin, M. and Hines, A.: Sea ice concentration and motion assimilation in a sea
394   ice−ocean model, J. Geophys. Res., 113(C5), C05S91, doi:10.1029/2007JC004224, 2008.
395   Tang, Q., Zhang, X., and Francis, J. A.: Extreme summer weather in northern midlatitudes linked to a
396   vanishing cryosphere, Nature Clim. Change, 4 (1): 45–50, 2014.
397   Tietsche, S., Notz, D., Jungclaus, J., and Marotzke, J.: Assimilation of sea-ice concentration in a global climate
398   model- physical and statistical aspects, Ocean Sci. 9(1): 19-36, 2013.
399   Vaughan, D.G., Comiso, J.C., Allison, I., Carrasco, J., Kaser, G., Kwok, R., Mote, P., Murray, T., Paul, F, Ren,
400   J., Rignot, E., Solomina, O., Steffen, K. and Zhang, T. : Observations: Cryosphere. In: Climate Change
401   2013: The Physical Science Basis. Contribution of Working Group I to the Fifth Assessment Report of
402   the Intergovernmental Panel on Climate Change [Stocker, T.F., Qin, D., Plattner, G.-K., Tignor, M.,
403   Allen, S.K., Boschung, J., Nauels, A., Xia, Y., Bex, V. and Midgley, P.M. (eds.)]. Cambridge University
404   Press, Cambridge, United Kingdom and New York, NY, USA, 2013.
405   Yang, S., and Christensen, J. H. : Arctic sea ice reduction and European cold winters in CMIP5 climate
406   change experiments, Geophys. Res. Lett., 39, L20707, doi:10.1029/2012GL053338, 2012.
407   Yang, Q., Losa, S. N., Losch, M., Jung, T., Nerger, L.: The role of atmospheric uncertainty in Arctic sea ice data
408   assimilation and prediction, Q. J. R. Meteorol. Soc., doi:10.1002/qj.2523, 2015a.
409   Yang, Q., Losa, S. N., Losch, M., Liu, J., Zhang, Z., Nerger, L., and Yang, H.: Assimilating summer sea ice
410   concentration into a coupled ice-ocean model using a localized SEIK filter, Ann. Glaciol., 56(69), doi:
411   10.3189/2015AoG69A740, 2015b.
412
413
414

415

416 Table 1. RMSE of the four forecasting experiments from mean ice thickness calculated by the ULS moorings
417 BGEP_2010A, BGEP_2010D and the satellite ice concentration observations. The two values refer to the
418 calculation using two different data sets SICCI-NSIDC.
419

|		BGEP_2010A	BGEP_2010D
1	MITgcm	0.86-0.89 m	0.93-0.97 m
2	LSEIK-1	0.43-0.46 m	0.55-0.59 m
3	LSEIK-2	0.61-0.64 m	0.51-0.55 m
4	LSEIK-3	0.43-0.46 m	0.59-0.62 m

420

421

422
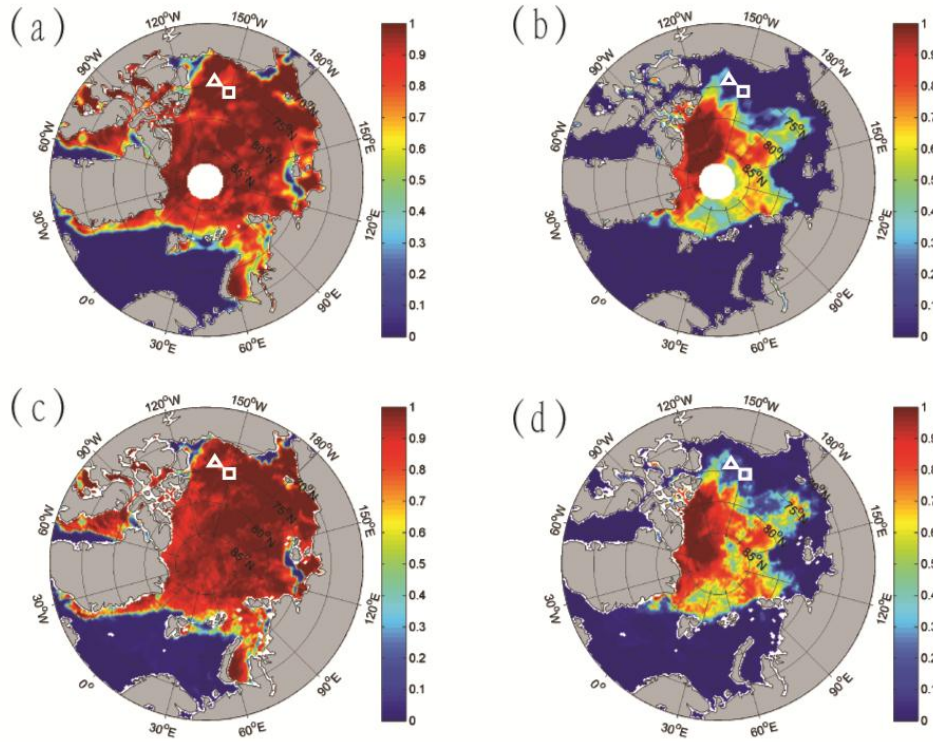
423
424 Figure 1. The NSIDC (a, b) and SICCI (c, d) sea ice concentration on 1 June (a, c) and 30 August 2010
425 (b, d). The locations of BGEP_2009A and BGEP_2009D are shown as a square with white line and a
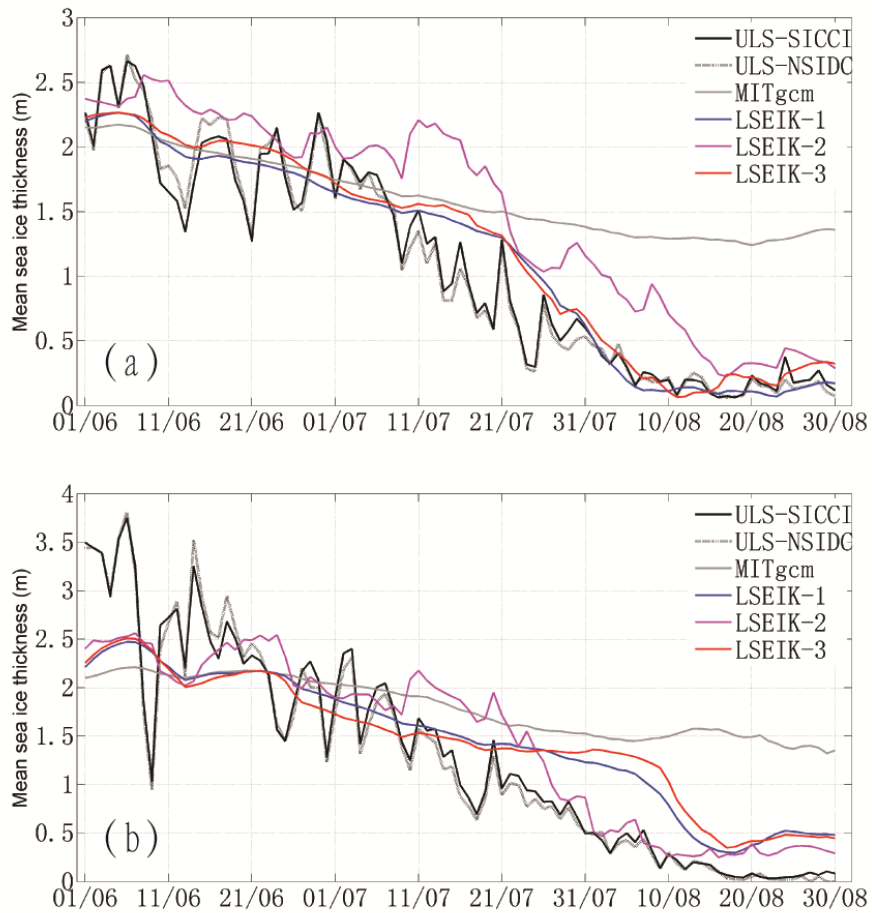426 triangle with white line, respectively.
427
428
429
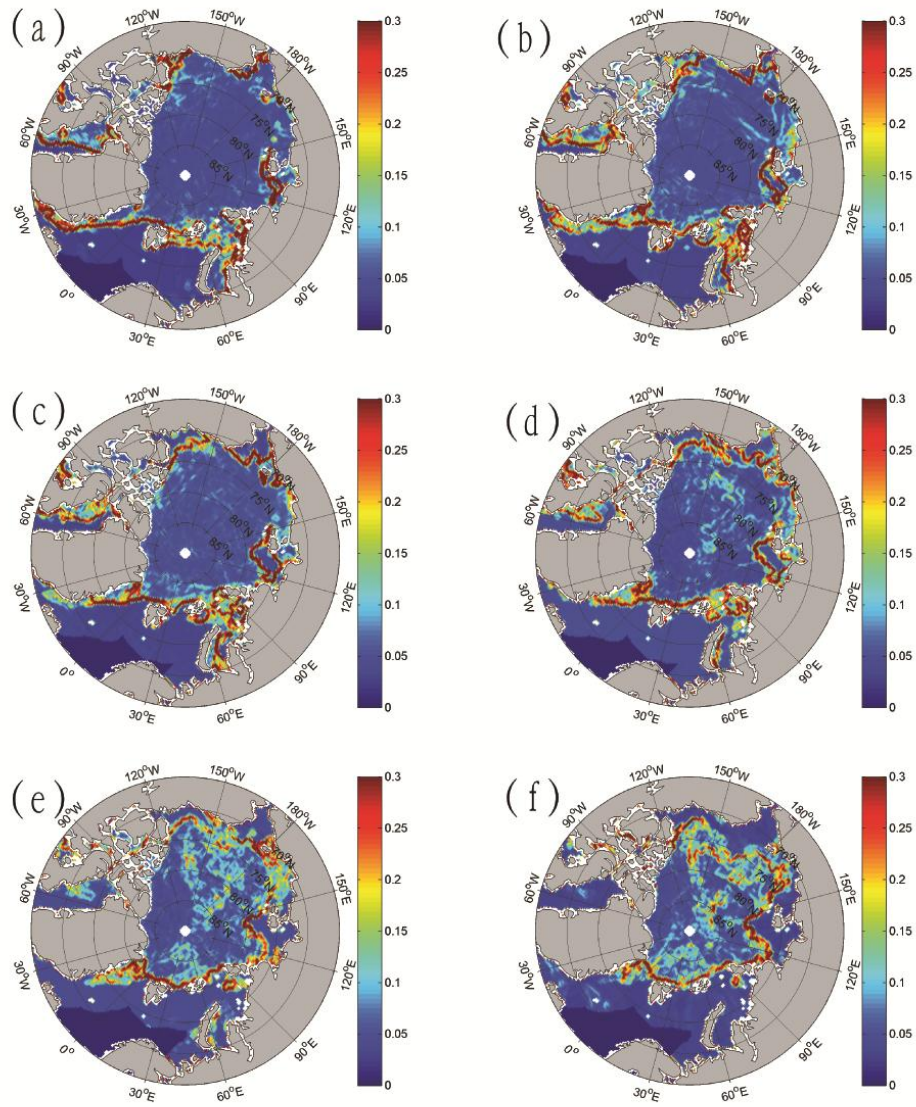
433
Figure 2. The SICCI sea ice concentration uncertainty on (a) 1 June, (b) 16 June, (c) 1 July, (d) 16 July,
(e) 1 August and (f) 16 August, 2010.

436
437

438

(a)
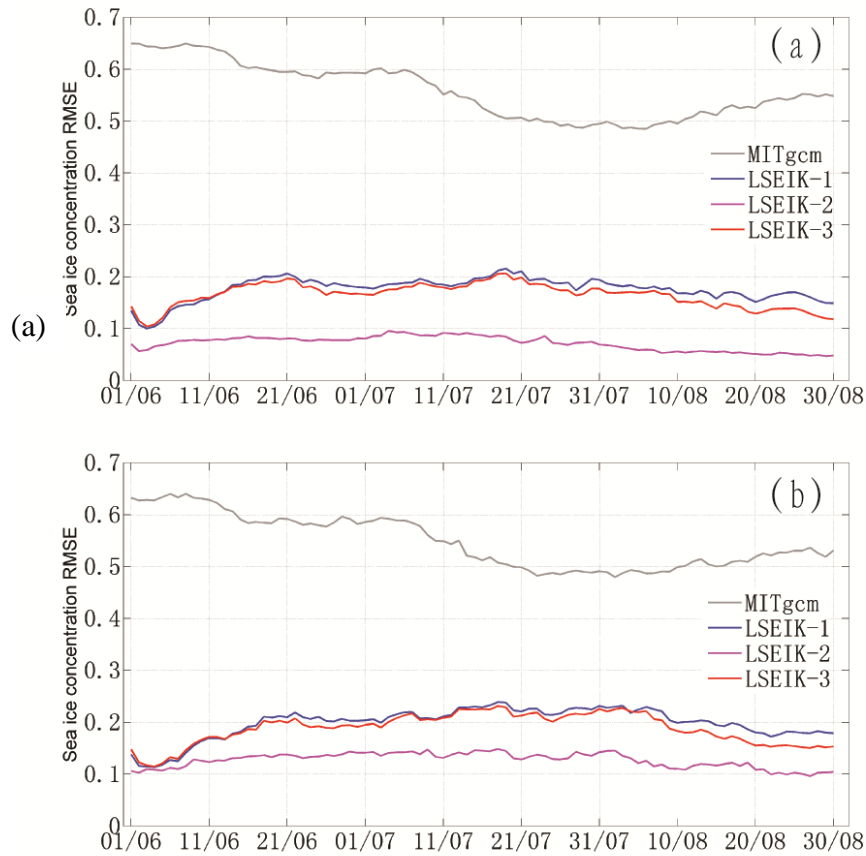
439
440
441   Figure 3.Temporal evolution of RMSE differences between sea ice concentration forecasts and the
442   SICCI (a) and NSIDC (b) ice concentration data. The RMSE of the MITgcm free-run, LSEIK-1,
443   LSEIK-2 and LSEIK-3 24-h forecasts are shown as gray, blue, magenta and red solid lines,
444   respectively.
445
446

447

448
449 Figure 4. Evolution of mean sea ice thickness (m) at (a) BGEP_2009A and (b) BGEP_2009D
450 Beaufort Sea from 1 June to 30 August 2010. The black solid and dashed lines show the obtained
451 mean ice thickness using SICCI and NSIDC sea ice concentrations, respectively. The MITgcm
452 free-run, LSEIK-1, LSEIK-2 and LSEIK-3 24 h ice thickness forecasts are shown as gray, blue,
453 magenta and red solid lines, respectively.
454

455
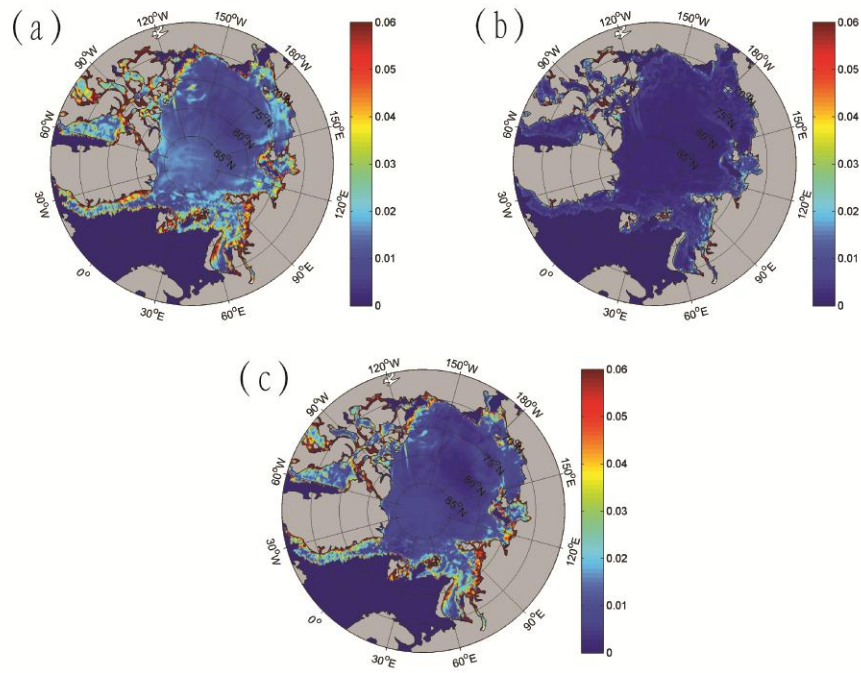
456
457   Figure 5. Sea ice-concentration standard deviation for the individual grid cells as calculated from the
458   24-h ensemble forecasts on 30 August 2010. (a) LSEIK-1, (b) LSEIK-2, and (c) LSEIK-3.
459
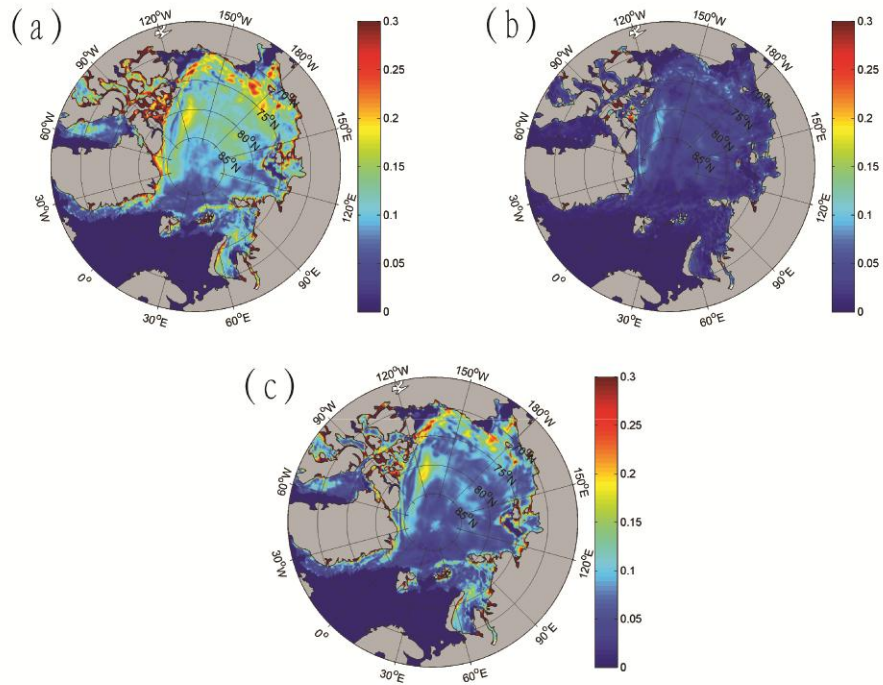
462
463 Figure 6. Sea ice thickness standard deviation for the individual grid cells as calculated from the 24-h
464 ensemble forecasts on 30 August 2010. (a) LSEIK-1, (b) LSEIK-2, and (c) LSEIK-3.
465